OPEN

Small Cell Neuroendocrine Carcinoma of Paranasal Sinuses: Radiologic Features in 14 Cases

Naier Lin, MD, Meng Qi, MD, Zhengyue Wang, MD, Siqi Luo, MD, Yucheng Pan, MD, Fang Zhang, MD, and Yan Sha, MD

Purpose: The purpose of this study was to explore the characteristic computed tomography (CT) and magnetic resonance (MR) features of small cell neuroendocrine carcinoma (SNEC) of paranasal sinuses.

Materials and Methods: Computed tomography (n = 8) and MR (n = 14) images and clinical findings from 14 patients with SNEC of paranasal sinuses were retrospectively reviewed.

Results: Eight lesions were located in the ethmoidal sinus, 4 in the maxillary sinus, and 2 in the sphenoid sinus. Small cell neuroendocrine carcinoma of the sphenoid sinus showed bilateral asymmetry patterns. On CT images, bony changes were visible in all 8 cases. On MR, 4 cases contained hemorrhage, and 10 cases contained cystic or necrotic areas. All cases demonstrated marked heterogeneous enhancement, with half showing a "cribriform-like" or "geographic" appearance. The nasal cavity was the most common site invaded by SNEC of paranasal sinuses, followed by the orbits. A time-signal intensity curve examination showed a washout-type pattern in all but 1 case. The mean ± SD apparent diffusion coefficient value was 0.702 ± 0.112 ($\times 10^{-3}$ mm^2/s). According to the Dulguerov staging system, 9 tumors were staged as N0 (1 T1, 1 T2, 5 T3, and 2 T4). The recurrence rate was 64.3%.

Conclusions: Some characteristics of radiological findings can provide important clues for preoperative diagnosis.

Key Words: small cell neuroendocrine carcinoma, neoplasm, computed tomography, magnetic resonance imaging, nasal cavity, paranasal sinus

(*J Comput Assist Tomogr* 2021;45: 135–141)

Neuroendocrine carcinoma (NEC) has an epithelial or a neural origin[1] and is represented by a spectrum of histologies, including low-grade carcinoids, intermediate-grade atypical carcinoids and high-grade small cell neuroendocrine carcinoma (SNEC).[2,3] Of these, SNEC is the most common histology with aggressive nature and high recurrence potential. There are a number of reports on SNEC in the gastrointestinal tract and lungs in the literature, but reports on paranasal sinuses involvement are rare. Until now, reports on sinonasal SNEC have mostly been limited to case reports or studies focused on treatment and pathologic diagnosis.[4–8]

Modern radiological imaging plays a revolutionary role in sinonasal tumor diagnosis and staging by providing clear information about tumor invasion in key anatomical structures, such as the skull base, orbit, and intracranial compartment. Furthermore, functional magnetic resonance (MR) technologies, such as diffusion-weighted imaging (DWI) and dynamic contrast-enhanced (DCE) imaging, have shown promising results in the differentiation of sinonasal tumors. Given the highly aggressive and recrudescent nature of SNEC, it is necessary to make correct preoperative diagnosis and staging to plan appropriate therapy. However, studies on the predictive role of radiologic features of SNEC of paranasal sinuses are lacking.[9,10]

The present study retrospectively analyzed computed tomography (CT) and MR imaging findings of 14 primary SNEC cases in paranasal sinuses as well as differential diagnostic considerations to determine whether there are distinct radiologic characteristics indicative of different diagnostic approaches.

MATERIALS AND METHODS

This retrospective study was approved by the institutional review board of our hospital. Between March 2014 and November 2018, data from 14 patients with histopathologically confirmed SNEC in paranasal sinuses were retrospectively reviewed. Computed tomography/MRI was performed within half a month before surgical resection. Before studying the images, informed consent was obtained from every participant.

Computed tomography images were obtained in 8 patients using a multislice helical CT system (SOMATOM; Siemens Medical, Erlangen, Germany) in both axial and coronal planes (voltage, 120 kV; current, 200 mA; thickness, 1.5 mm; exposure time, 5.8 seconds). Enhanced images were obtained 45 to 50 seconds after the intravenous administration of a nonionic contrast agent (Iopamidol, 100 mL; injection rate, 2 mL/s; BeiLu Pharmaceutical Co, Beijing, China).

Magnetic resonance imaging was performed in all of the patients using a 3-T Siemens MRI system (Magnetom Verio or Prisma; Siemens Medical, Erlangen, Germany) with a 12-channel head coil. For conventional MRI, nonenhanced axial turbo spin-echo (TSE) T1-weighted imaging (T1WI) (repetition time/echo time [TR/TE] range, 349 milliseconds/9.1 milliseconds; slice thickness, 5 mm), and axial and coronal fat-saturated TSE T2-weighted imaging (T2WI) (TR/TE, 3780 milliseconds/101 milliseconds; thickness, 5 mm) were performed. Diffusion-weighted MRI was performed using a high-resolution DWI system (readout-segmented echo-planar imaging, parallel imaging, 2-dimensional navigator-based reacquisition; number of segments, 5; TR/TE, 4700 milliseconds/66 milliseconds; *b* values, 0, 1000 s/mm^2; thickness, 4 mm; number of diffusion directions, 3). After the intravenous administration of Gd-DTPA (Magnevist, Bayer Schering, Berlin, Germany; 0.1–0.2 mmol/kg body), fat-saturated T1-weighted TSE images were obtained in axial and coronal planes (TR/TE, 4700 milliseconds/66 milliseconds; thickness, 4 mm; matrix, 192 × 192; field of view, 24 cm × 24 cm). The DCE time-signal intensity curve (TIC) examination was performed in 5 cases (3-dimensional fast low-angle shot sequence; TR/TE, 7.52 milliseconds/2.06 milliseconds; section thickness, 5 mm; field of view, 220 × 220; temporal

From the Department of Radiology, Eye & ENT Hospital, Fudan University, Shanghai, China.

Received for publication February 2, 2020; accepted May 14, 2020.

Correspondence to: Yan Sha, MD, Department of Radiology, Eye and Ear, Nose and Throat Hospital, Shanghai Medical College, Fudan University, 83 Fenyang Rd, Shanghai, 200031, China (e-mail: yanshavip@yeah.net).

The authors declare no conflict of interests.

This study was approved by the Ethics Committee of the Eye and Ear, Nose and Throat Hospital of Fudan University.

DOI: 10.1097/RCT.0000000000001065

resolution, 7 s/dynamic; number of dynamics, 30; total scanning time, 3 minutes 43 seconds].

All of the lesions were evaluated by 2 radiologists who reached a consensus with regard to tumor location, margin definition, extension, enhancement, and bony structural changes. On CT and MR images, the enhancement degree was categorized as moderate, approaching the adjacent muscle, or marked, approaching the nasal mucosa. Apparent diffusion coefficient (ADC) maps were constructed from high-resolution diffusion-weighted images (b = 0, 1000 s/mm^2). When measuring the ADC value of lesions, the region of interest was carefully placed in the solid portion of the tumor, avoiding cystoid variation, hemorrhage, and necrosis. The TIC patterns were categorized as persistent type (continuous increase in signal intensity), plateau type (maximum signal intensity reached within 1 minute; washout ratio, 10%–20%), or washout type (maximum signal intensity reached within 1 minute; washout ratio, >20%).[11]

The inspection reports of conventional microscopic hematoxylin-eosin staining and immunohistochemical (IHC) data of all the lesions were collected. The IHC staining markers included neuron-specific enolase (NSE), chromogranin A (CgA), synaptophysin (Syn), cytokeratin (CK), thyroid transcription factor 1, S-100, epithelial membrane antigen, and vimentin.

According to the modified Kadish classification system,[12] SNEC cases were staged as follows: A, lesion limited to the nasal cavity; B, lesion limited to the sinonasal tract; C, lesion extending beyond the sinonasal tract; and D, lesions with cervical or distant metastasis. In addition, the Dulguerov staging system for sinonasal malignancies with neuroendocrine differentiation, which uses the TNM classification and includes the imaging data, was used in our cohort (Table 1).[13]

RESULTS

The median age of the patients at the time of diagnosis was 52 years (range, 38–82 years) with a slight male predilection (8 males and 6 females). The general clinical manifestations included nasal obstruction, epistaxis or rhinorrhea, exophthalmos, and headache. The symptoms lasted from 1 month to 6 months.

Of the 14 lesions, 8 were primarily located in the ethmoidal sinus (Figs. 1–3), 4 in the maxillary sinus (Fig. 4), and 2 in the sphenoid sinus (Fig. 5). Five cases were on the left side (Figs. 1, 2), 6 cases were on the right side (Figs. 4, 6), and the other 3 cases were bilateral (Figs. 3, 5). Both the SNEC cases in the sphenoid sinus showed bilateral asymmetrical patterns (Fig. 5).

The radiologic imaging features for our cohort are summarized in Table 2. All of the lesions were irregularly shaped with ill-defined borders. In the 8 patients who underwent a CT scan, the tumors appeared isodense. Bony changes, including bony absorption and evasion (n = 8) (Figs. 1A, 4A) or reactive sclerosis (n = 2), were observed in our series. After the administration of contrast, the tumor showed moderate (n = 7) or marked (n = 1) enhancement. Moreover, the necrotic or cystic areas were observed in 5 cases (Fig. 1A).

On MRI, tumors appeared isointense on T1WI and heterogeneous on T2WI. Four cases contained hyperintense areas on both T1WI and T2WI (Figs. 3A, B), consistent with hemorrhage. Eleven cases contained scattered cystic or necrotic areas with high signal within the tumor on T2WI (Fig. 1B). After the administration of DTPA, tumors showed moderate (n = 6) (Figs. 1C, 2) or marked (n = 8) (Figs. 4B, 5A, 5B, 6A) heterogeneous enhancement, and 50% (7/14) of SNEC cases had a typical "cribriform-like" or "geographic" enhancement appearance, especially in the ethmoidal sinuses (Figs. 1C, 2). The DCE TIC showed the washout-type pattern in all but 1 case. On DWI, the mass demonstrated a hyperintense signal and significant hypointense ADC signal (Figs. 1D, 5C). The mean $ADC_{b0,\ 1000}$ value in our cohort was 0.702 ± 0.112 ($\times 10^{-3}$ mm^2/s).

The aggressive nature of tumors was demonstrated by invasion into adjacent structures beyond the paranasal sinuses, including the nasal cavity (n = 14), orbits (n = 9), superior/inferior orbital fissure (n = 5), optic canal (n = 3), pterygopalatine fossa (n = 7), foramen rotundum (n = 2), foramen ovale (n = 2), pterygoid canal (n = 1), infratemporal fossa (n = 2), skin of the nose or cheek (n = 3), cavernous sinus (n = 4), pharyngonasal cavity (n = 4), parapharyngeal space (n = 3), and brain (n = 3) (Fig. 6).

Histopathologically, SNEC consists of sheets and cords of small-sized cells with little cytoplasm. Necrotic areas are frequently observed, varying from scattered, individual necrotic cells to confluent geographic areas of necrosis. Immunohistochemical characteristics demonstrated consistent positive staining for CK and Syn and negative staining for S-100 and thyroid transcription factor 1 in all tumors. Furthermore, in the majority (more than 50%) of cases, the staining for CgA, NSE, and epithelial membrane antigen was positive, whereas that for vimentin and P63 was negative.

According to the modified Kadish classification system, the stage distribution in our series was as follows: 1 case with stage B, 8 cases with stage C, and 5 cases with stage D disease. According to the Dulguerov staging system, the SNEC tumors in our cohorts were distributed as follows: 1 T1, 1 T2, 8 T3, and 4 T4. Five cases were considered to have cervical lymph node metastasis on both radiological findings and neck pathological examination (staged as N1). Lung metastases were found in 1 patient at the time of diagnosis (staged as M1), but no other distant metastases were found in our cohort.

TABLE 1. Dulguerov Staging System

Staging	Description
Primary tumor	
T1	Tumor involving the nasal cavity and/or paranasal sinuses (excluding sphenoid), sparing the most superior ethmoid
T2	Tumor involving the nasal cavity and/or paranasal sinuses (including sphenoid) with extension to or erosion of the cribriform plate
T3	Tumor extension into the orbit or protruding into the anterior cranial fossa, without dural involvement
T4	Tumor involving the brain
Lymph nodes	
N0	No cervical lymph node metastasis
N1	Any form of cervical lymph node metastasis
Distant metastasis	
M0	No metastasis
M1	Distant metastasis

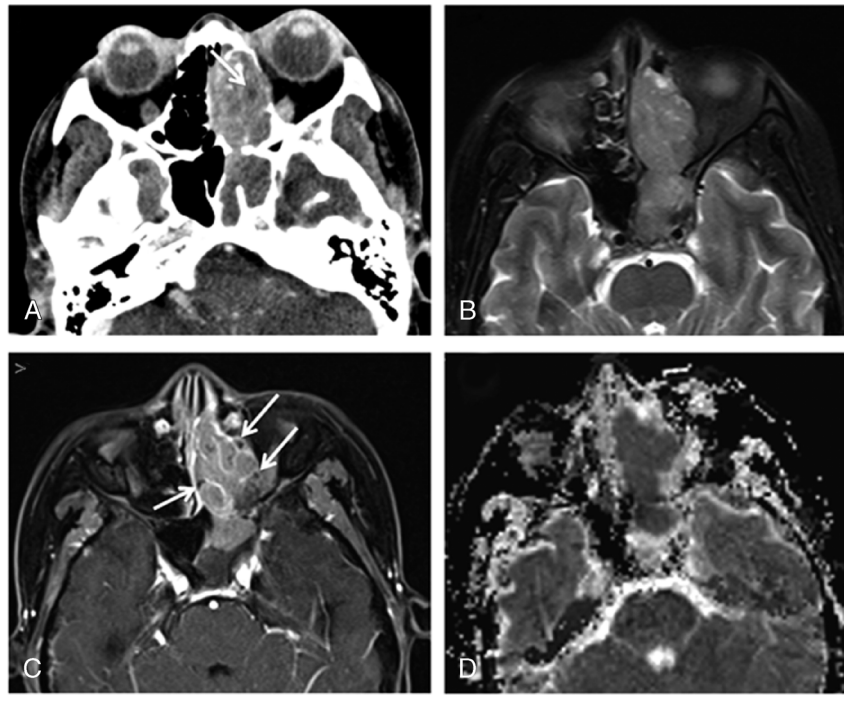

FIGURE 1. Computed tomography and MRI of 52-year-old woman with tumor in the left ethmoidal sinus diagnosed as SNEC. A, Axial enhanced CT image reveals ill-defined expansile mass with moderate enhancement in left ethmoidal sinus and extending into nasal cavity and sphenoid sinus. The necrotic or cystic areas within tumor (arrow) and adjacent bony erosion are observed. B, Tumor on axial fat-saturated T2-weighted image shows isointense. C, Axial enhanced magnetic resonance image reveals moderate enhancement with cribriform-like appearance (arrows) of tumor. D, The ADC map revealed the significantly low mean ADC value of 0.591×10^{-3} mm^2/s.

All of the patients underwent surgery and radiotherapy, and 5 patients received adjuvant chemotherapy before or after the surgery. During 3 months to 3 years of follow-up, tumor recurrence occurred in 9 cases (64.3%). Three patients with T4 stage disease (1 each T4N1M0, T4N1M1, and T4N0M0) died during the follow-up period.

DISCUSSION

Small cell neuroendocrine carcinoma occurs mainly in the lungs, and extrapulmonary SNEC represents only 4% of all SNEC cases.[14] Small cell neuroendocrine carcinoma of paranasal sinuses is extremely rare, and the first case was described by Raychowdhuri[15] in 1965. Until now, less than 100 cases have been published in the literature. It has been postulated that, as a NEC, SNEC is derived from neuroendocrine amine precursor uptake and decarboxylation cells, which are widely distributed in the body.[2] Based on IHC analysis, the tumors show characteristic immune reactivity for neuroendocrine differentiation markers, such as CK, CgA, Syn, and NSE.

Small cell neuroendocrine carcinoma is more common in middle-aged and elderly adults, and the average age of incidence is approximately 50 years.[7] Some reports have described this tumor to display no sex predilection,[7] whereas a slight male predominance was identified by Han et al[4] in a review of 54 sinonasal SNEC

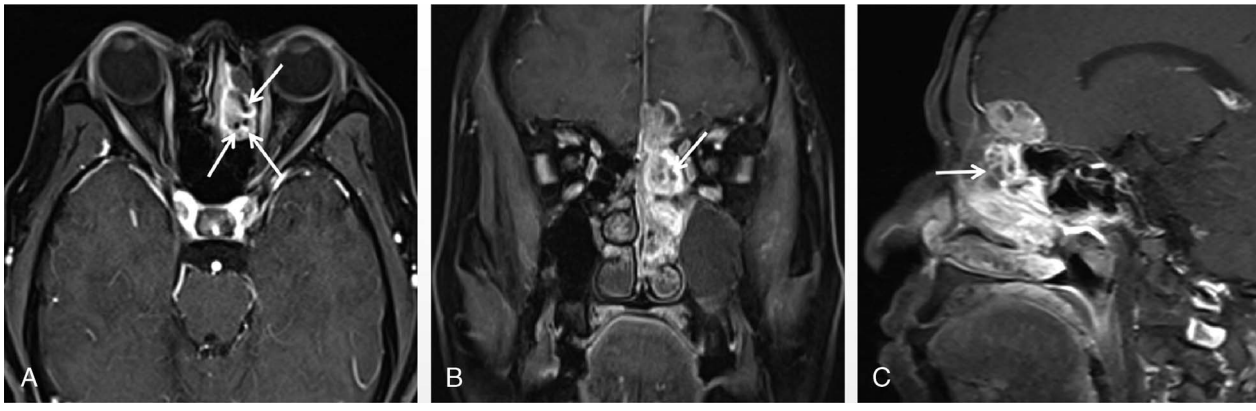

FIGURE 2. A 62-year-old man with tumor in left ethmoid sinus. The tumor was histologically diagnosed as SNEC. A, Axial enhanced MRI, (B) coronal enhanced MR, and (C) sagittal enhanced MR images reveal the heterogeneously enhanced mass with cribriform-like appearance (arrows).

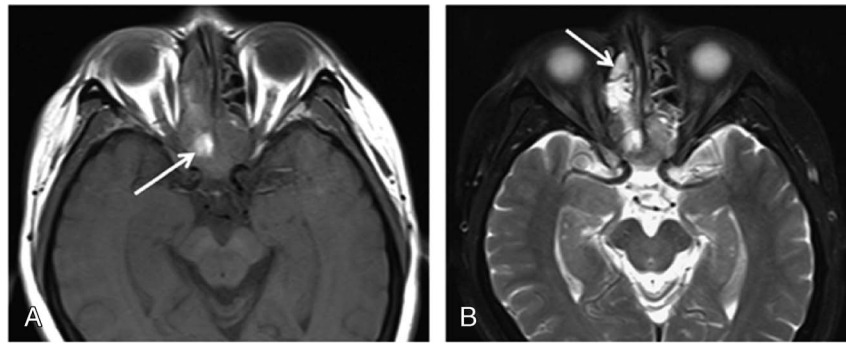

FIGURE 3. Magnetic resonance imaging of 59-year-old man with pathologically diagnosed SNEC in bilateral posterior ethmoid sinuses and extending into sphenoid sinuses. A., Tumor demonstrates isointense on T1-weighted image with the hyperintensity areas consistent with hemorrhage (arrow). B, On fat-saturated T2-weighted image, tumor shows heterogeneously isointense and hyperintense; the retained secretions in the right anterior ethmoid sinus show high signal (arrow).

lesions. Our study was in line with the review by Han (showing 8 males and 6 females). Although SNEC tumors may produce ectopic hormones, the clinical manifestations of hormone production were not observed in our study, and the symptoms were nonspecific.

The diagnosis of SNEC is based on the pathological features of the specimen obtained by surgical resection; however, radiological examination can enable preoperative diagnosis, which is better for early staging and treatment planning. Unlike other types of sinonasal carcinoma, which are most commonly observed in maxillary sinuses, in the present and previous studies,[4,10] the predominant site of SNEC lesions was ethmoid sinuses, followed by maxillary sinuses. Zhu et al[9] proposed a bilateral symmetry or "pigeon" pattern as a characteristic of SNEC in sphenoid sinuses; however, in our series, both SNEC lesions in sphenoid sinuses showed bilateral but asymmetric patterns.

On unenhanced CT, tumors tended to show isoattenuation, and after administration of the contrast agent, mild or moderate enhancement was observed with hypointense areas, indicating necrosis and cysts. Calcification is uncommon in SNEC, which was consistent with previous studies.[9,10] Computed tomography is useful for assessing the bony involvement of the anterior skull base, ethmoid sinus, frontal bone, sphenoid bone, and orbit. Bony changes, especially bony absorption and erosion, were observed in all cases in our series.

Magnetic resonance imaging assesses the intrinsic characteristics of SNEC much better than CT. Typically, the lesions present with ill-defined borders, heterogeneous isointense, or slight hyperintense T2 signals with frequent cystic changes and marked enhancement after the administration of DTPA. In addition, a typical cribriform-like or geographic enhancement appearance was observed in half of our cases, especially those in ethmoidal sinuses. This feature is correlated with histopathologically scattered necrotic cells or geographic necrotic areas within the tumor and could be an important clue for aiding diagnosis. In addition, MRI can be useful to better identify tumor extent and invasion into adjacent tissues. Similar to that in a study of 19 cases by Zhu et al,[9] the nasal cavity was the most common site invaded by SNEC of paranasal sinuses in our study, followed by the orbits, pterygopalatine fossa, superior/inferior orbital fissure, cavernous sinus, and pharyngonasal cavity.

Dynamic contrast-enhanced MRI has been applied to distinguish sinonasal lesions and provide information about microcirculation in tumors for decades; however, to the best of our knowledge, there are no data about TIC characteristics of sinonasal SNEC. In our series, all cases demonstrated enhancement with an immediate rapidly progressive linear increase in signal intensity followed by washout TIC type in 4 lesions and plateau type in 1, demonstrating that SNEC is a hypervascular malignancy with increased vessel density and high vascular permeability.

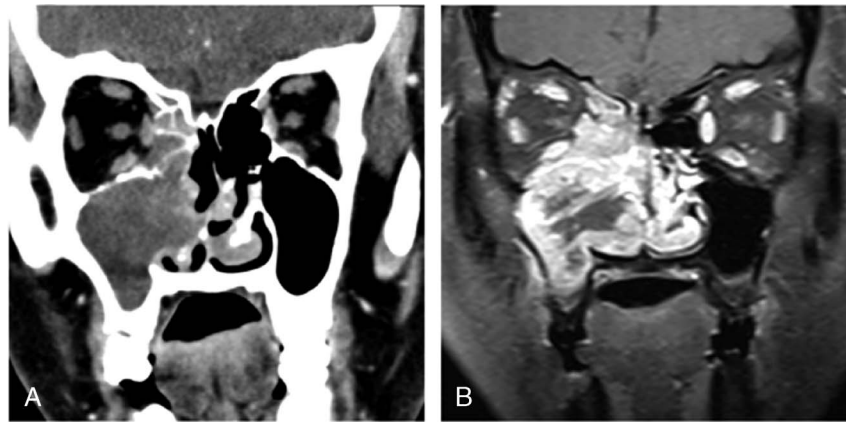

FIGURE 4. Computed tomography and MRI of 50-year-old woman with pathologically diagnosed SNEC in right maxillary sinus. A, Coronal CT image shows that tumor has moderate enhancement and extending into nasal cavity, ethmoid sinus, and orbit. B, Coronal contrast-enhanced MR image reveals heterogeneous markedly enhanced tumor with necrotic areas.

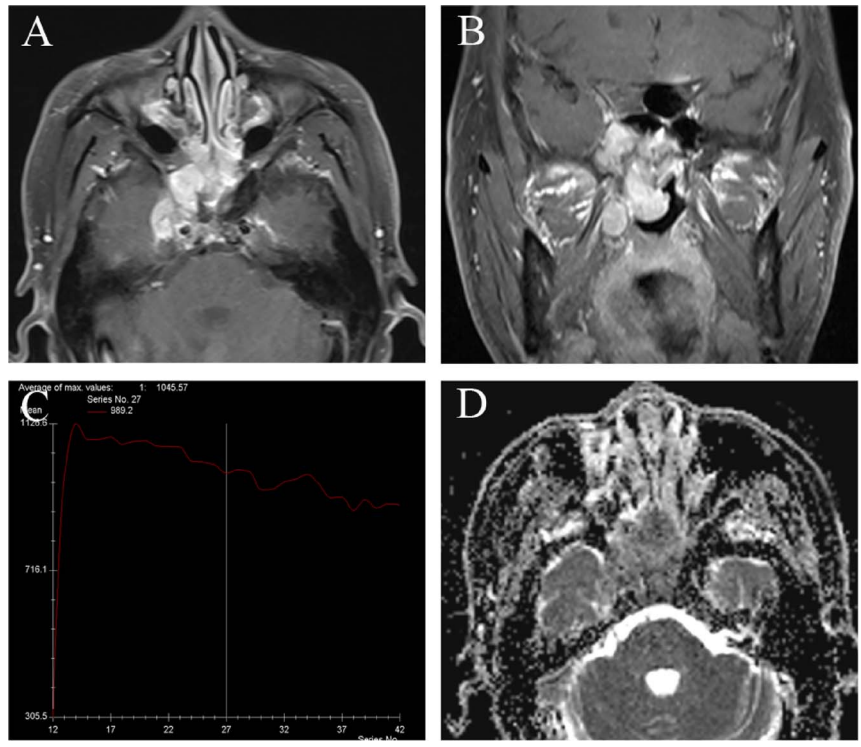

FIGURE 5. Magnetic resonance imaging of 49-year-old man with SNEC in bilateral sphenoid sinuses. A, Axial enhanced MRI and (b) coronal enhanced MR image reveal the markedly enhanced tumor in sphenoid sinuses. Tumor shows bilateral asymmetry pattern and extending to bilateral nasal choana, right foramen ovale, and cavernous sinus. (C) The TIC examination revealed washout type. D, The ADC map revealed the mean ADC value of 0.724×10^{-3} mm^2/s.

Diffusion-weighted imaging is a functional MRI technique that reflects the free movement of water molecules in tissues. Until now, there is only 1 study by Gencturka et al[16] that described the significant restriction of diffusion inside of NEC. In that study, they calculated the quantitative DWI parameters, including ADCmean and ADCratio, and revealed a low ADC value for sinonasal NEC (0.45 ± 0.29 [$\times 10^{-3}$ mm^2/s]). In our study, we used high-resolution DWI (RESOLVE) with ADC mapping in SNEC cases and observed a low ADC mean value of 0.702 ± 0.112 ($\times 10^{-3}$ mm^2/s), consistent with the nature of increased cellularity and reduced extracellular space in SNEC lesions as well as a consequent decrease in water molecule diffusivity.

In our series, 2 cases of sinonasal SNEC involving the anterior cranial fossa were misdiagnosed as olfactory neuroblastoma (ONB). As the most common type of neuroendocrine tumor, ONB is characterized by intracranial extension through the skull base, and a previous study[17] suggested the location of the typical waist of ONB lesions on the cribriform plate, representing a "dumbbell" shape; however, this feature was not observed in SNEC.

Another case of SNEC in sphenoid sinuses (Fig. 5) was misdiagnosed as adenoid cystic carcinoma (ACC), as the lesion involved the right pterygopalatine fossa and foramen ovale, which consequently widened the foramen ovale with heavy enhancement.

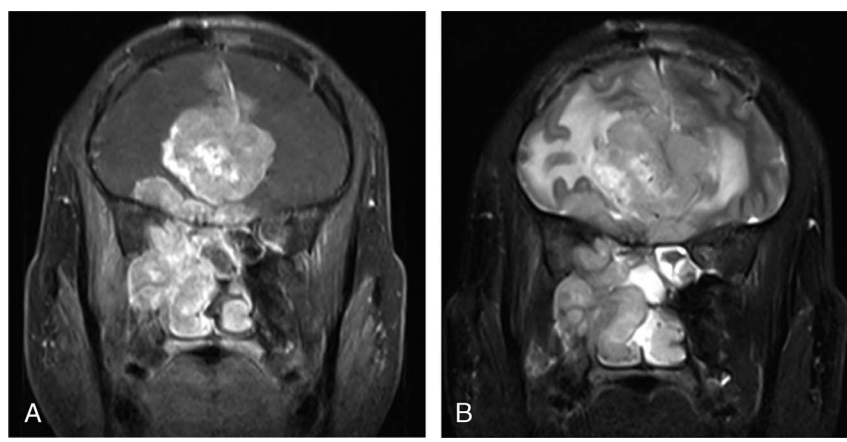

FIGURE 6. Magnetic resonance imaging of 39-year-old man who presented with recurrent right nasal hemorrhage and nasal congestion. The tumor was histologically diagnosed as SNEC. A, Coronal contrast-enhanced MR image reveals ill-defined mass filling the right maxillary sinus and nasal cavity, and extending into orbit and intracranially. B, Coronal T2-weighted image shows peritumoral cyst.

TABLE 2. The Radiologic Imaging Features of SNEC of Paranasal Sinuses

						CT			MRI						Clinical Outcome (3 mo to 3 y)	
Case	CT/MRI	Location	R/L/B	Modified Kadish	Dulguerov Staging	Density	Enhancement	Bony Change	Hemorrhage	Necrosis	Enhancement	Cribriform-Like or Geographic Feature	TIC Type	$ADC_{b0,100}$ Value, $\times 10^{-3}$ mm^2/s	Recurrence	Vital Status
1	CT/MRI	Ethmoidal sinus	L	C	T3N0M0	Isodense	Moderate	Yes	No	Yes	Moderate	Yes		0.591	None	Alive
2	CT/MRI	Maxillary sinus	R	C	T4N0M0	Isodense	Marked	Yes	Yes	Yes	Marked	No		0.684	Local	Dead of disease
3	MRI	Ethmoidal sinus	L	B	T1N0M0				No	Yes	Moderate	Yes	Plateau	0.631	None	Alive
4	CT/MRI	Maxillary sinus	R	D	T3N1M0	Isodense	Moderate	Yes	No	No	Marked	No	Washout	0.527	Local	Alive
5	MRI	Ethmoidal sinus	B	C	T3N0M0				Yes	Yes	Marked	No		0.599	Local	Alive
6	MRI	Ethmoidal sinus	R	D	T3N1M0				No	No	Marked	Yes	Washout	0.774	Local	Alive
7	CT/MRI	Maxillary sinus	R	D	T4N1M0	Isodense	Moderate	Yes	No	Yes	Marked	No		0.809	Local	Dead of disease
8	MRI	Ethmoidal sinus	L	C	T2N0M0				No	Yes	Moderate	No		0.776	None	Alive
9	CT/MRI	Sphenoid sinus	B	C	T3N0M0	Isodense	Moderate	Yes	No	No	Marked	No	Washout	0.724	Local	Alive
10	MRI	Ethmoidal sinus	L	C	T3N0M0				No	Yes	Moderate	Yes		0.947	None	Alive
11	MRI	Maxillary sinus	R	D	T4N1M1				Yes	Yes	Marked	Yes	Washout	0.628	Local and distant	Dead of treatment complications
12	CT/MRI	Ethmoidal sinus	L	C	T4N0M0	Isodense	Moderate	Yes	No	Yes	Moderate	Yes		0.743	Local	Alive
13	CT/MRI	Sphenoid sinus	B	D	T3N1M0	Isodense	Moderate	Yes	No	Yes	Moderate	Yes		0.615	None	Alive
14	CT/MRI	Ethmoidal sinus	R	C	T3N0M0	Isodense	Moderate	Yes	Yes	Yes	Marked	No		0.782	Local	Alive

R indicates right; L, left; B, bilateral.

Although ACC is well known for its propensity for perineural extension, which appears as a replacement of fat in the neural foramina and pathologic enhancement and thickening of the involved cranial nerves, these features are not specific.[16] In addition, the higher signal intensity on T2WI and higher ADC value of ACC than those of other malignancies, such as NEC, squamous cell carcinoma, and lymphoma,[16] could facilitate differential diagnosis.

In a study on sinonasal NEC by Likhacheva et al,[18] only 8% of patients had lymph node metastasis, which was significantly lower than that for nonsinonasal NEC cases of the head and neck.[19] In the present study, SNEC in paranasal sinuses had a higher incidence of cervical lymphadenopathy than that in the report by Likhacheva et al,[18] accounting for 35.7% (5/14) of the cases, which could have resulted from the higher invasiveness of SNEC cases in our study.[10]

Key anatomical structure involvement is often related to poor prognosis. Although the modified Kadish system, the most widely used staging system for NEC, typically allows for staging using radiological data before treatment, it has been criticized because, even at the same stage, prognosis is completely different between patients with and without brain involvement. Thus, based on the TNM classification, the Dulguerov staging system is preferable for sinonasal malignancies with neuroendocrine differentiation by some authors because this system recognizes the early involvement of the cribriform plate as the T2 stage and separates intracranial but extradural lesions from those with true brain involvement, thus benefiting treatment decisions. In our series, 4 patients with intracranial extension were diagnosed with T4-stage disease.

Although management of sinonasal SNEC requires complete surgical resection with clear margins, the presence of an extensive high-grade tumor makes complete surgical resection impossible. Hence, adjuvant nonsurgical therapy is often necessary to enhance the local control rate, and follow-up is very important for monitoring the course of disease. Unfortunately, we did not have long-term follow-up data in the present study. The recurrence of SNEC in our series was high at 64.3% during 3 to 30 months, close to the rate (reaching 70% at 3 years) described by Silva et al.[20] In addition, all 3 patients who died had T4-stage disease, revealing a significantly high invasiveness of tumor involving the brain.

There are several limitations in our study. First, the rarity of SNEC of paranasal sinuses has made large-scale studies on the radiological features difficult. Second, although our study used functional MRI methods, more advanced MRI techniques such as quantitative DCE, intravoxel incoherent motion DWI, and diffusion kurtosis imaging would provide additional information. Thus, we emphasize the need for further studies on larger cohorts with more functional imaging methods to better explore this rare sinonasal tumor.

CONCLUSIONS

The diagnosis of SNEC is challenging, and this disease can easily be misdiagnosed; familiarity with the characteristic imaging features of this rare tumor could help in preoperative diagnosis and staging. Small cell neuroendocrine carcinoma should be considered when the patient presents with an ill-defined tumor in paranasal sinuses (especially in ethmoidal sinuses) and heterogeneous or typical cribriform-like or geographic enhancement, together with invasion into the nasal cavity, orbit, and anterior and middle cranial fossa. The final diagnosis should be made based on histopathological immunohistochemistry.

ACKNOWLEDGMENTS

The entire article has been revised and edited by American Journal Experts Language Editing Services.

RREFERENCES

1. Chang ED, Kim MK, Kim JS, et al. Primary neuroendocrine tumor of the breast: imaging features. *Korean J Radiol*. 2013;14:395–399.
2. Rosenthal DI, Barker J, El-Naggar AK, et al. Sinonasal malignancies with neuroendocrine differentiation: patterns of failure according to histologic phenotype. *Cancer*. 2004;101:2567–2573.
3. Weinreb I, Perez-Ordonez B. Non-small cell neuroendocrine carcinoma of the sinonasal tract and nasopharynx. Report of 2 cases and review of the literature. *Head Neck Pathol*. 2007;1:21–26.
4. Han G, Wang Z, Guo X, et al. Extrapulmonary small cell neuroendocrine carcinoma of the paranasal sinuses: a case report and review of the literature. *J Oral Maxillofac Surg*. 2012;70:2347–2351.
5. Faisal M, Haider I, Adeel M, et al. Small cell neuroendocrine carcinoma of nose and paranasal sinuses: the Shaukat Khanum Memorial Cancer Hospital experience and review of literature. *J Pak Med Assoc*. 2018;68: 133–136.
6. Gonzalez-Garcia R, Fernandez-Rodriguez T, Naval-Gias L, et al. Small cell neuroendocrine carcinoma of the sinonasal region. A propose of a case. *Br J Oral Maxillofac Surg*. 2007;45:676–678.
7. Babin E, Rouleau V, Vedrine PO, et al. Small cell neuroendocrine carcinoma of the nasal cavity and paranasal sinuses. *J Laryngol Otol*. 2006; 120:289–297.
8. Ma AT, Lei KI. Small cell neuroendocrine carcinoma of the ethmoid sinuses presenting with generalized seizure and syndrome of inappropriate antidiuretic hormone secretion: a case report and review of literature. *Am J Otolaryngol*. 2009;30:54–57.
9. Zhu Q, Zhu W, Wu J, et al. The CT and MRI observations of small cell neuroendocrine carcinoma in paranasal sinuses. *World J Surgical Oncology*. 2015;13:54–58.
10. Zhou C, Duan X, Liao D, et al. CT and MR findings in 16 cases of primary neuroendocrine carcinoma in the otolaryngeal region. *Clin Imag*. 2015;39: 194–199.
11. Yang B, Wang Y, Wang S, et al. Magnetic resonance imaging features of schwannoma of the sinonasal tract. *J Comput Assist Tomogr*. 2015;39: 860–865.
12. Morita A, Ebersold MJ, Olsen KD, et al. Esthesioneuroblastoma: prognosis and management. *Neurosurgery*. 1993;32:706-715.
13. Dulguerov P, Calcaterra T. Esthesioneuroblastoma: the UCLA experience 1970-1990. *Laryngoscope*. 1992;102:843–849.
14. Ibrahim NB, Briggs JC, Corbishley CM. Extrapulmonary oat cell carcinoma. *Cancer*. 1984;54:1645–1661.
15. Raychowdhuri RN. Oat cell carcinoma and paranasal sinuses. *J Laryngol Otol*. 1965;79:253–255.
16. Gencturka M, Ozturka K, Caicedo-Granados E, et al. Application of diffusion-weighted MR imaging with ADC measurement for distinguishing between the histopathological types of sinonasal neoplasms. *Clin Imag*. 2019;55:76–82.
17. Dublin A, Bobinski M. Imaging characteristics of olfactory neuroblastoma (esthesioneuroblastoma). *J Neurol Surg B*. 2016;77:1–5.
18. Likhacheva A, Rosenthal DI, Hanna E, et al. Sinonasal neuroendocrine carcinoma: impact of differentiation status on response and outcome. *Head Neck Oncol*. 2011;3:32.
19. Barker JL, Glisson BS, Garden AS, et al. Management of nonsinonasal neuroendocrine carcinomas of the head and neck. *Cancer*. 2003;98: 2322–2328.
20. Silva EG, Butler JJ, Mackay B, et al. Neuroblastomas and neuroendocrine carcinomas of the nasal cavity: a proposed new classification. *Cancer*. 1982;50:2388–2405.